INTERNATIONAL JOURNAL FOR NUMERICAL METHODS IN FLUIDS
Int. J. Numer. Meth. Fluids 2001; **37**: 865–884 (DOI: 10.1002/fld.174)

A new stable space–time formulation for two-dimensional and three-dimensional incompressible viscous flow

Donatien N'dri[a], André Garon[b,*,1] and André Fortin[c]

[a] *Département de Mathématiques et de Génie Industriel, École Polytechnique de Montréal, Montréal, Québec, Canada*
[b] *Département de Génie Mécanique, École Polytechnique de Montréal, Montréal, Québec, Canada*
[c] *Département de Mathématiques et de Statistiques, Université Laval, Cité Universitaire Québec, Montréal, Québec, Canada*

SUMMARY

A space–time finite element method for the incompressible Navier–Stokes equations in a bounded domain in $\mathbb{R}^d$ (with $d = 2$ or 3) is presented. The method is based on the time-discontinuous Galerkin method with the use of simplex-type meshes together with the requirement that the space–time finite element discretization for the velocity and the pressure satisfy the inf–sup stability condition of Brezzi and Babuška. The finite element discretization for the pressure consists of piecewise linear functions, while piecewise linear functions enriched with a bubble function are used for the velocity. The stability proof and numerical results for some two-dimensional problems are presented. Copyright © 2001 John Wiley & Sons, Ltd.

KEY WORDS: inf–sup condition; Navier–Stokes equations; space–time

1. INTRODUCTION

The solution of time-dependent problems such as the incompressible Navier–Stokes equations by finite element methods leads to the mixing of finite elements in space and finite differences in time. In contrast, the space–time formulation performs the discretizations in space and time concurrently by blending the space and time variables into a space–time finite element. This space–time element has one extra dimension, and the finite element interpolation functions are dependent on both the space and time variables. In other words, this procedure can be viewed as an extension of the finite element method over the time domain.

* Correspondence to: Département de Génie Mécanique, École Polytechnique de Montréal, CP 6079, Succ. centre-ville Montréal, Québec, H3C 3A7, Canada.
[1] E-mail: andreg@meca.polymtl.ca

Received 15 May 2000
Revised 11 December 2000

Although the concept was originally introduced by Oden [1] and Fried [2], the first numerical results can be traced back to Bonnerot and Jamet [3,4] for the Stefan problem. Improving on the time-continuous interpolation used in their previous formulation, Jamet [5] later introduced another approach. His idea was to permit the unknown to be discontinuous with respect to time. This procedure, known as the time-discontinuous Galerkin method, allows the space–time domain to be organized into a series of 'slabs' $S_n = \Omega \times (t_n, t_{n+1})$, where Ω is the underlying spatial domain and t_n is a discrete time level. The fully discretized equations are then solved on one space–time slab at a time, leading to a time-marching procedure in which the solution for the current slab provides the initial condition for the next one.

The time-discontinuous Galerkin method has been successfully applied to numerous problems such as heat conduction [3,6], elastodynamics structural [7–9], acoustics [10–12], etc. Unfortunately, like the standard Galerkin method, the time-discontinuous Galerkin method has been shown to produce spurious numerical oscillations in convection-dominated problems.

To eliminate these oscillations, Varoglu and Finn [13,14] first employed the method of characteristics to modify the spatial discretization at each time step. Johnson and Saranen [15], and Hansbo and Szepessy [16] introduced the streamline diffusion (SD) method. These formulations enhance stability through the addition of a small least-squares term to the test functions. Tezduyar and Behr [17,18] presented the Galerkin least-squares space–time (GLS/ST) method, which is obtained by adding a least-squares term to the discrete equation, which is proportional to the equation residual. This kind of method falls into the category of stabilization techniques.

In the case of the incompressible Navier–Stokes equations, we also have in addition to the spurious oscillations due to the convection-dominated flows, the problem of choosing the test spaces for the pressure and the velocity in such a way that no instability occurs. In other words, the approximation spaces for velocity and pressure must *a priori* satisfy a compatibility condition known as the inf–sup condition, also referred to in the literature as the LBB condition by Ladyzhenskaya [19], Babuška [20] and Brezzi [21]. Hughes [22] pointed out that the stabilized formulations can also be used with approximation spaces that do not satisfy the LBB condition. This led to the use of stabilizing techniques based on equal order interpolation. However, to our knowledge, there is no published work on the construction of approximation spaces for velocity and pressure that satisfy the LBB condition in the context of the space–time finite element methods.

The development of a stable, mixed space–time finite element is the goal of this paper. We first present the Navier–Stokes equations and then the time-discontinuous Galerkin method, followed by a brief review of the inf–sup condition and its extension to space–time formulations. The full description of our element and the stability proof are then presented next, and the paper concludes with some two-dimensional numerical examples.

2. GOVERNING EQUATIONS

We consider a viscous, incompressible Newtonian fluid occupying at time instant $t \in (0, T)$ a bounded region $\Omega \subset \mathbb{R}^d$, with boundary $\Gamma = \partial\Omega$. The primary degrees of freedom are $\boldsymbol{u}(\boldsymbol{x}, t)$, the velocity of the fluid and the pressure $p(\boldsymbol{x}, t)$. The conservation of mass and momentum of the fluid are expressed by the equations

$$\nabla \cdot \boldsymbol{u} = 0 \quad \text{on } \Omega, \quad \forall t \in (0, T) \tag{1}$$

and

$$\rho\left(\frac{\partial \boldsymbol{u}}{\partial t} + (\boldsymbol{u} \cdot \nabla)\boldsymbol{u} + \boldsymbol{f}\right) - \nabla \cdot \boldsymbol{\sigma} = 0 \quad \text{on } \Omega \quad \forall t \in (0, T) \tag{2}$$

where ρ is the density of the fluid, $\boldsymbol{f}$ is a volume force and $\boldsymbol{\sigma}$ is the Cauchy stress tensor defined by

$$\boldsymbol{\sigma} = -p\mathbf{I} + 2\mu\varepsilon(\boldsymbol{u})$$

The strain tensor ε is related to the velocity field by the relation

$$\varepsilon(\boldsymbol{u}) = \frac{1}{2}(\nabla \boldsymbol{u} + (\nabla \boldsymbol{u})^T)$$

and μ is the viscosity of fluid. These equations are commonly referred to as the Navier–Stokes equations.

Along with these equations, proper boundary conditions must be imposed. Boundary conditions for the Navier–Stokes equations are of two types. If the velocity is prescribed on Γ, the condition is said to be essential

$$\boldsymbol{u} \cdot \boldsymbol{e}_i = \boldsymbol{g}_i \quad \text{on } (\Gamma_D)_i \quad \forall t \in (0, T), \quad i = 1, d \tag{3}$$

If normal stress is prescribed, we speak of a natural boundary condition

$$\mathbf{n} \cdot \boldsymbol{\sigma} \cdot \boldsymbol{e}_i = \mathbf{h}_i \quad \text{on } (\Gamma_N)_i \quad \forall t \in (0, T), \quad i = 1, d \tag{4}$$

where $\mathbf{n}$ is an outward unit normal to the boundary Γ of Ω, $\{\boldsymbol{e}_i\}_{i=1}^d$ is a basis in $\mathbb{R}^d$, and $(\Gamma_D)_i$ and $(\Gamma_N)_i$ are complementary subsets of Γ in relation to the Dirichlet and Neumann condition for each of the velocity components. The initial condition consists of a divergence-free velocity field specified over the entire initial domain. This condition is given by

$$\boldsymbol{u}(\boldsymbol{x}, 0) = \boldsymbol{u}_0 \quad \text{on } \Omega \tag{5}$$

In our case, $\boldsymbol{u}_0 = 0$.

3. THE TIME-DISCONTINUOUS GALERKIN METHOD

The time-discontinuous Galerkin method is a space–time finite element method for parabolic and hyperbolic (first- or second-order) problems. This approach is based on the use of finite element discretizations in space and time concurrently with basis functions that are continuous

in space and discontinuous at the discrete time levels. It has been shown that this method possesses considerable advantages not available in traditional semi-discrete approaches (finite elements in space, finite differences in time). Indeed, the time-discontinuous Galerkin method often leads to A-stable, higher-order implicit time stepping schemes (optimal for parabolic problems [6,23–25] or nearly optimal for hyperbolic problems [8,26]) which are suitable for the development of various types of adaptative procedures [8,24,27–29]. Finally, moving or free boundaries can be handled without unnecessary technical difficulties [6,17,18,30].

3.1. Variational formulation

To define the method, we consider an ordered partition of the open time interval $I = (0, T)$ into subintervals $I_n = (t_n, t_{n+1})$, where t_n and t_{n+1} belong to an ordered series of time steps $0 = t_0 < t_1 < t_2 \cdots < t_N = T$. Let $\Sigma_n = \partial\Omega \times I_n$ and $\Omega_n = \Omega \times \{t_n\}$. We then define the space–time slab S_n as the domain enclosed by the surfaces Ω_{n+1}, Ω_n and Σ_n (see Figure 1). In order to apply Dirichlet or Neumann conditions, the surface Σ_n can be decomposed into two complementary subsets Σ_{D_n} and Σ_{N_n}, with a decomposition for each of the velocity components which may be different. Within each space–time element, the trial and weighting functions are polynomials in $\boldsymbol{x}$ and t. These functions are assumed to be $C^0(S_n)$, i.e. continuous throughout each space–time slab, but are allowed to be discontinuous across the interfaces of the slabs. The discontinuity of the finite element functions across space–time slab interfaces provides the possibility of changing the mesh from one slab to the next, orienting the mesh along characteristic [13,31–37] or according to *a posteriori* error estimates, which increases precision and permits larger time steps.

For each space–time slab S_n, $n = 0, 1, \ldots, N-1$, let V_n^h and Q_n^h be the finite dimensional spaces of the underlying velocity and pressure function spaces $X = (H^1_{\Sigma_D}(S_n))^d$ and $Q = L^2(S_n)$. The type of element and the choice of V_n^h and Q_n^h are the subject of the next section.

The space–time variational formulation is obtained from a weighted residual of the governing Equations (1) and (2) within a space–time slab and incorporates time-discontinuous jump terms across slab interfaces.

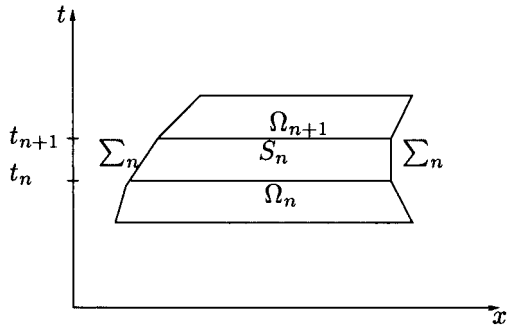

Figure 1. Space–time slab.

Within each space–time slab S_n, $n = 0, 1, \ldots, N-1$, the space–time formulation can be written as follows: given $\mathbf{u}^n_-$, find $\mathbf{u}^h \in V^h_n$ and $p^h \in Q^h_n$ such that $\forall \mathbf{v}^h \in V^h_n$, $\forall q^h \in Q^h_n$

$$\int_{S_n} \rho\left(\frac{\partial \mathbf{u}^h}{\partial t} + \mathbf{u}^h \cdot \nabla \mathbf{u}^h + \mathbf{f}\right) \cdot \mathbf{v}^h \, \mathrm{d}\Omega \, \mathrm{d}t + \int_{S_n} 2\mu\varepsilon(\mathbf{u}^h) : \varepsilon(\mathbf{v}^h) \, \mathrm{d}\Omega \, \mathrm{d}t - \int_{S_n} p \nabla \cdot \mathbf{v}^h \, \mathrm{d}\Omega \, \mathrm{d}t$$
$$- \int_{\Sigma_{N_n}} \mathbf{h} \cdot \mathbf{v}^h \, \mathrm{d}\Gamma + \int_{S_n} q^h \nabla \cdot \mathbf{u}^h \, \mathrm{d}\Omega \, \mathrm{d}t + \int_{\Omega_n} \rho(\mathbf{u}^n_+ - \mathbf{u}^n_-) \cdot \mathbf{v}^n_+ \, \mathrm{d}\Omega = 0 \tag{6}$$

where $\mathbf{u}^n_\pm = \lim_{\varepsilon \to 0} \mathbf{u}^h(t_n \pm \varepsilon)$.

In the variational formulation given by (6), the first five terms constitute the standard Galerkin formulation of the problem. The last one is the time-discontinuous jump term integral on slab interfaces Ω_n. This jump term transports the data from slab to slab via an L^2 projection.

4. PRESENTATION OF THE ELEMENT

It is well known that the mixed Galerkin formulation suffers from stability problems when the combination of the interpolations for the velocity and pressure spaces does not satisfy the inf–sup condition (see Brezzi–Fortin [38]). The numerical consequence of not satisfying this condition appears as oscillations in the pressure field, which are referred to as 'spurious pressure modes'.

Before presenting our space–time element, we discuss the inf–sup condition in the context of the space–time finite element methods.

4.1. The inf–sup condition

To introduce the inf–sup condition, let T_h be a triangulation of Ω so that h denotes the mesh size parameter.

Mathematical analysis of the Stokes problem has shown that the well-posedness of the Galerkin formulation of the steady state Stokes problem is governed by the inf–sup condition [19–21]: there exists a constant α independent of h such that

$$\inf_{\mathbf{Q}_h} \sup_{\mathbf{V}_h} \frac{\int_\Omega q_h \nabla \cdot \mathbf{v}_h}{\|\mathbf{v}_h\|_V \|q_h\|_Q} \geq \alpha > 0 \tag{7}$$

where V_h and Q_h are finite dimensional subspaces of the underlying velocity and pressure functions spaces, $V = (H^1_0(\Omega))^d$ and $Q = L^2_0(\Omega)$.

From the variational formulation of the continuity equation (1), we introduce the bilinear form $b(\,.\,,\,.\,)$ on $X \times M$ such that

$$b(\mathbf{v}, q) = \int_{S_n} q \nabla \cdot \mathbf{v} \, \mathrm{d}\Omega \, \mathrm{d}t = \int_{I_n} \int_\Omega q \nabla \cdot \mathbf{v} \, \mathrm{d}\Omega \, \mathrm{d}t$$

where the divergence operator is defined only with respect to spatial variables

$$\left(\nabla\cdot\mathbf{u}=\frac{\partial u}{\partial x}+\frac{\partial v}{\partial y}\right)$$

Together with the notations used in (6) and following the inf–sup condition of the form $b(\,.\,,\,.\,)$, the inf–sup condition in the context of space–time can be formulated as follows: there exists a constant α independent of h such that

$$\inf_{\mathbf{Q}_h}\sup_{\mathbf{v}_h}\frac{\int_{S_n} q_h\nabla\cdot\mathbf{v}_h}{\|\mathbf{v}_h\|_V\|q_h\|_Q}\geq\alpha>0 \tag{8}$$

where V_h and Q_h are finite dimensional subspaces of the underlying velocity and pressure function spaces, $X=(H^1_{\Sigma_n}(S_n))^d$ and $M=L^2_0(S_n)$.

4.2. The space–time mini-tetrahedral element

When implementing the space–time formulation, the elements will become one dimension higher to account for the time dimension. We note two classes of space–time elements: extruded elements (comprising quadrilaterals, prisms, bricks, etc.) formed by a straightforward extrusion of the spatial element in the time dimension, and simplex elements comprising triangles, tetrahedra, etc. In this study, we chose the simplex-type element, which leads to the use of completely unstructured meshes within the space–time slab and the possibility of having a different mesh at the bottom and at the top the space–time slab, thereby avoiding grid-to-grid interpolation when remeshing occurs.

From Arnold–Brezzi–Fortin [39], it is well known that enriching the velocity approximation space either by adding standard or inter-edge or inter-face bubble functions often leads to stability. This fundamental idea will also be true in the context of space–time finite elements methods. First let's describe the simplest stable element of this kind, which we referred to here as the space–time mini-element.

A discretization of the space–time slab is performed by partitioning S_n into tetrahedral elements (see Figure 3). For a given tetrahedron K, using the standard finite element notation, we denote as space–time mini the element consisting of piecewise linear functions enriched with a bubble function for the velocity and piecewise linear functions for the pressure. The bubble function is piecewise linear on each K_i, $i=1, 2, 3, 4$, where K_1, K_2, K_3, K_4 are the four subtetrahedra obtained by connecting the barycenter of K with its vertices (see Figure 2). In order to define the finite element spaces of the underlying element, we set

$$B_1(K)=\{b\in H^1_{\Sigma_n}(S_n),\ |b|_{K_i}\in P_1(K_i)\cap H^1_0(K),\ K\in T_h\ \ (i=1, 2, 3, 4)\}$$

and we have

$$V_h=\{\boldsymbol{v}_h\in(C^0(S_n))^d|\boldsymbol{v}_h|_K\in(P_1(K))^d\ \ \forall K\}\oplus(B_1(K))^d$$

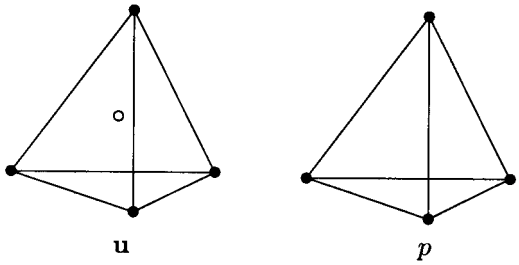

Figure 2. Mini-element.

$$Q_h = \{q_h \in (C^0(S_n)) | q_n|_K \in (P_1(K)) \ \forall K\}$$

Remark 1
In contrast, with the standard mini-three-dimensional element, this element has 10 degrees of freedom (two per node) for the velocity instead of 15 (three per node).

Remark 2
The space–time mini-element presented above has a three-dimensional counterpart, which consists of this extension to hyper-tetrahedra.

4.3. Stability proof for the space–time mini-element

We consider in this section the proof of the inf–sup condition for the mini-element. The most general way to do this is to build some interpolation operator Π_h satisfying Fortin's criteria [38]. First, let us recall the Fortin's criteria and some related results.

Proposition 1
If we can construct an operator

$$\begin{aligned} \Pi_h: \quad & V \to V_h \\ & \boldsymbol{u} \mapsto \Pi_h \boldsymbol{u} \end{aligned}$$

satisfying

$$\int_\Omega \nabla \cdot (\boldsymbol{u} - \Pi_h \boldsymbol{u}) q_h \, d\Omega = 0, \quad \forall q_h \in Q_h \tag{9}$$

and

$$\|\Pi_h \boldsymbol{u}\|_V \leq c\|\boldsymbol{u}\|_V, \quad c > 0 \tag{10}$$

with c independent of h and $\|\ \|_V$ the norm on V, then the discrete inf–sup condition holds.

In some cases, Fortin [40] suggests to build the operator in two steps, summarize in the following proposition.

Proposition 2
Let $\Pi_1 \in \mathscr{L}(V, V_h)$ and $\Pi_2 \in \mathscr{L}(V, V_h)$ be such that

$$\|\Pi_1 \boldsymbol{v}\|_V \leq c_1\|\boldsymbol{v}\|_V, \quad \forall \boldsymbol{v} \in V \tag{11}$$

$$\|\Pi_2(I - \Pi_1)\boldsymbol{v}\|_V \leq c_2\|\boldsymbol{v}\|_V, \quad \forall \boldsymbol{v} \in V \tag{12}$$

$$\int_\Omega \nabla\cdot(\boldsymbol{v} - \Pi_2 \boldsymbol{v}) q_h \, \mathrm{d}\Omega = 0, \quad \forall \boldsymbol{v} \in V, \quad \forall q_h \in Q_h \tag{13}$$

where constants c_1 and c_2 are independent of h. If we set

$$\Pi_h \boldsymbol{u} = \Pi_1 \boldsymbol{u} + \Pi_2(\boldsymbol{u} - \Pi_1 \boldsymbol{u}) \tag{14}$$

then the inf–sup condition holds.

In the case of continuous pressure, Π_1 will be the interpolation operator of Clément [41] which satisfies for $v \in H^1(\Omega)$

$$\sum_K h_K^{2m-2}|\boldsymbol{v} - \Pi_1 \boldsymbol{v}|^2_{m,K} \leq c\|\boldsymbol{v}\|^2_{1,\Omega}, \quad m = 0, 1 \tag{15}$$

The interpolation operator of Clément which is also referred to a local regularization operator of Clément, is a continuous interpolate using average values of v instead of pointwise values. It is constructed via a local projection. Such operators were originally introduced for triangular meshes by Clément in [41], extended to quadrilateral meshes by Fortin [40] and generalized by Bernardi [42] to treat (isoparametric) d-simplices (triangles, tetrahedral, hypertetrahedral). We also refer to the recent work of Bernardi–Girault [43] for the state of the art in the construction of such operators.

The operator Π_2 on the other hand is constructed on each element K, in order to satisfy (13) and in many cases, with the additional requirement that

$$\|\Pi_2 \boldsymbol{v}\|_{1,K} \leq c(h_K^{-1}\|\boldsymbol{v}\|_{0,K} + |\boldsymbol{v}|_{1,K}) \tag{16}$$

We can summarize these results in the following proposition.

Proposition 3
Let V_h be such that a 'Clément's operator': Π_1: $V \to V_h$ exists and satisfies (15). If we can construct an operator: Π_2: $V \to V_h$ such that (13) and (16) hold, then the operator Π_h defined by (14) satisfies (9) and (10) and, therefore, the discrete inf–sup condition holds.

After these preparations, we are ready for the main result of this paper, which is summarized in the following proposition.

Proposition 4
The space–time mini-element satisfies the 'inf–sup' condition.

The standard proof of the stability of mini-element (cf. Brezzi–Fortin [38]) applies quite directly, with minor changes due to the space–time nature of the element.

Proof
Let Π_1 be the operator of Clement. We refer to the work of Bernardi [42] for the existence and approximation result (15) in the case of tetrahedral and hypertetrahedral meshes. We have now to construct Π_2. Since in each element we have $\mathbf{v}_h \in (P_1(K))^d \oplus (B_1(K))^d$, we build Π_2: $V \to (B_1(K))^d$ and define it, on each K, as the solution of

$$\begin{cases} \Pi_2 \mathbf{v}|_K \in (B_1(K))^d \\ \displaystyle\int_K (\Pi_2 \mathbf{v} - \mathbf{v}) \, \mathrm{d}\Omega \, \mathrm{d}t = 0 \end{cases} \tag{17}$$

It is clear that (17) has a unique solution and since, $\Pi_2 \mathbf{v}|_K \in (B_1(K))^d$, which from a scaling argument (see Dupont–Scott [44]) yields the following inverse inequality:

$$\|\Pi_2 \mathbf{v}\|_{1,K} \leq c h_K^{-1} \|\mathbf{v}\|_{0,K}, \quad \forall \mathbf{v} \in V$$

where h_K is now a space–time mesh parameter, from which the temporal approximation enters implicitly into the stability proof. From the inverse inequality, (16) holds.

To check condition (13), we recall that the pressure is continuous (($Q_h \subset C^0(S_n)$)) hence we have

$$\int_{S_n} \nabla \cdot (\Pi_2 \mathbf{v} - \mathbf{v}) q_h \, \mathrm{d}\Omega \, \mathrm{d}t = \int_{I_n} \left(\int_\Omega \nabla \cdot (\Pi_2 \mathbf{v} - \mathbf{v}) q_h \, \mathrm{d}\Omega \right) \mathrm{d}t = - \int_{I_n} \int_\Omega (\Pi_2 \mathbf{v} - \mathbf{v}) \cdot \nabla q_h \, \mathrm{d}\Omega \, \mathrm{d}t$$

where the gradient and the divergence are defined only with respect to the spatial variables. By Fubini's theorem, the last integral is well defined with the requirement that $\mathbf{v} \in L^1(t_n, t_{n+1}; (H^1(\Omega))^d)$. Together with this weak regularity condition, we have

$$\int_{I_n}\int_{\Omega}(\Pi_2\mathbf{v}-\mathbf{v})\cdot\nabla q_h \,\mathrm{d}\Omega\,\mathrm{d}t=\int_{S_n}(\Pi_2\mathbf{v}-\mathbf{v})\cdot\nabla q_h \,\mathrm{d}\Omega\,\mathrm{d}t$$

Since we used a piecewise linear pressure field, the following is obtained:

$$\int_{S_n}(\Pi_2\mathbf{v}-\mathbf{v})\cdot\nabla q_h \,\mathrm{d}\Omega\,\mathrm{d}t=\sum_K\int_K(\Pi_2\mathbf{v}-\mathbf{v})\cdot\nabla q_h \,\mathrm{d}\Omega\,\mathrm{d}t=0$$

so that condition (13) is satisfied and the inf–sup condition holds. This proof is valid for two-dimensional and three-dimensional + *time* mini-elements.

Remark 3
Since the gradient operator is only defined with respect to the spatial variables, it is necessary for the approximation to be linear in space. But the only crucial requirement is that the $\nabla q_h \in (P_0(K))^d$ (constant by space–time element) which is not the case for extruded bi- or tri-linear elements.

5. NUMERICAL EXAMPLES

In this section, we present numerical examples in order to verify the stability of the mini-element and the effectiveness of the proposed formulation.

We have considered the computation of a Poiseuille flow, a no-flow test, a flow behind a circular cylinder, and Stokes's second problem. The first two tests are simple flow problems which admit steady-state solutions, but which are instructive in the context of incompressible flow problems [45]. The third leads to a transient solution and the development of a Von Karmann vortex street behind a circular cylinder. The last one involved the simulation of the flow over a moving domain.

5.1. Numerical methodology

Together with the complete definition of the interpolation spaces, the formulation (6) is solved sequentially for all space–time slabs, starting with the initial condition $\boldsymbol{u}^0_- = 0$. For each space–time S_n, $n = 0, 1, \ldots, N-1$, the computation of (6) results in a global non-linear system of algebraic equations which is solved iteratively using a quasi-Newton method, with numerical evaluation of the Jacobian matrices. The linearized systems are solved using a direct solver (LU decomposition). Meanwhile, it is worth mentioning that the bubble function is eliminated from the global system via *static condensation* in order to make the formulation competitive on a computational point of view.

Since remeshing is not an issue here, we consider the same spatial mesh for the top and the bottom of the space–time slab, so that the burden of the construction of the space–time mesh is restricted to the spatial mesh. This mesh is obtained by a straightforward extrusion of the spatial mesh formed by triangular elements. Then, the resulting six-node prism mesh is divided into tetrahedra (see Figure 3).

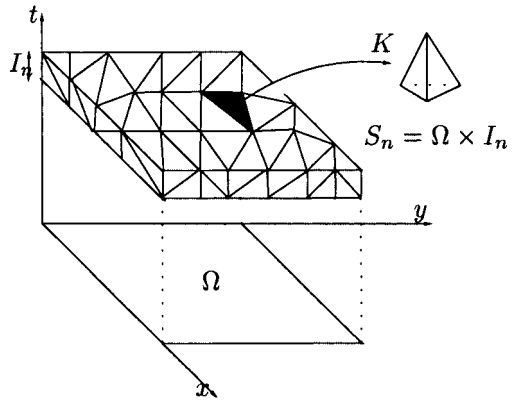

Figure 3. Discretization of the space–time slab.

5.2. The Poiseuille flow

A parabolic velocity profile is imposed at both the inlet and outlet of a rectangular channel and a no-slip condition is imposed on the parallel walls. A parabolic velocity profile and a linear pressure are the analytic solutions to the problem.

The mesh for this computation is illustrated in Figure 4. In order to show the numerical effect of not satisfying the inf–sup condition, we compare three elements: the tetrahedron $P_1 - P_0$ element (linear velocity, piecewise constant pressure), the (prism) $Q_1 - P_0$ element and the mini-space–time element.

Several methods have been proposed to arrive at an intuitive evaluation of the inf–sup condition. One of these is the constraint ratio. The computation of this ratio for our three elements with the given mesh (see Figure 4) leads us to reject the tetrahedron $P_1 - P_0$ element due to the fact that its ratio is greater than 1, which would lead to a *locking phenomenon*.

In our first attempt, we used the (prism) $Q_1 - P_0$ element. As we can see in Plates 1 and 2, the pressure field is subject to oscillations even though the velocity field is satisfactory. Next, we used the space–time mini-element, for which the results are satisfactory with a stable pressure field (see Plates 3 and 4).

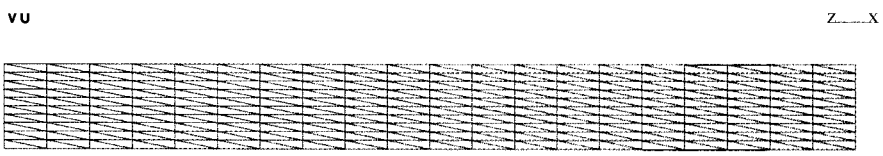

Figure 4. Mesh.

5.3. The no-flow test

The no-flow test was first considered by Gresho [46]. On the boundary of the computational domain, the x-component and the y-component of the velocity were specified to be zero. A non-zero external force $\mathbf{f} = (0, g)$ was imposed. The analytical solution is $\mathbf{u} = 0$ and the pressure solution is linear.

Plates 5–7 show that, using a coarse mesh the space–time mini-element passes the no-flow test, yielding the solution for both velocity and pressure. This result was expected due to the fact that this element is linear for both velocity and pressure.

5.4. Simulation of the Von Karmann vortex street behind a circular cylinder

The simulation of the Von Karman vortex street behind a circular cylinder has long been used as a benchmark problem to test the performance of numerical algorithms for solving the Navier–Stokes equations. We present numerical results for the flow behind a cylinder at a Reynolds number of 100.

Figure 5 illustrates the computational domain and boundary conditions. A free natural boundary conditions is weakly enforced at the outflow section. The Reynolds number is defined by $Re = DU/v$, where D is the diameter of the cylinder, U is the free-stream velocity and μ is the kinematic viscosity. Since both the diameter of the cylinder and the free-stream velocity were set to unity, the kinematic viscosity was set to 0.01 to achieve a Reynolds number of 100. A complete description of this problem can be found in Engelman and Jaminia [47].

The mesh used for this simulation was built using previous knowledge about the formation of the vortex street behind the cylinder: it is more refined in that area and the refinement is good enough to capture the unsteady structures of the flow at the Reynolds number of 100. The computation is started with a null initial condition with a fixed time step Δt set to 0.1.

Figure 6 is the time history of the y-component of the velocity reported at the location $(x = 4,\ y = 0)$ and shows the periodic behavior of the vertical velocity component. The frequency of the oscillations is in accordance with the benchmark solution [47]. The next results presented in Plates 8–13 are contour plots over the full domain of various quantities at

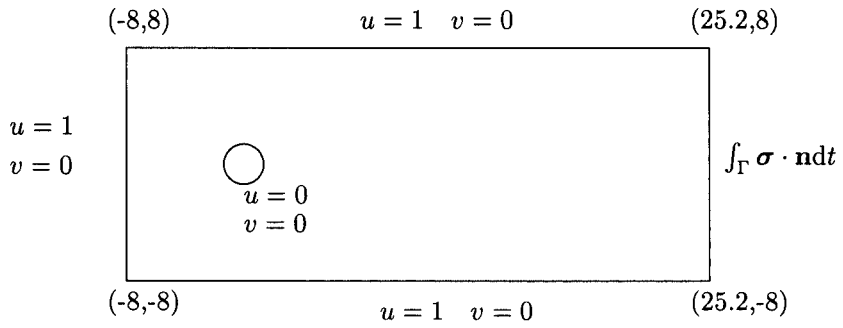

Figure 5. Computational domain and boundary conditions.

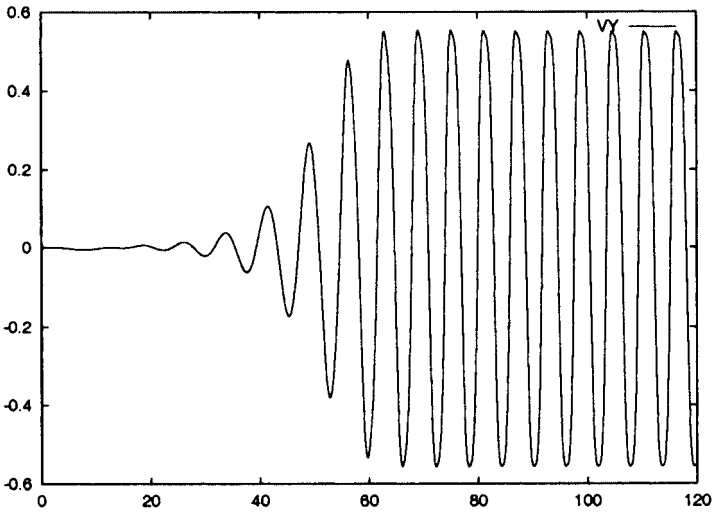

Figure 6. Time history of the y-velocity.

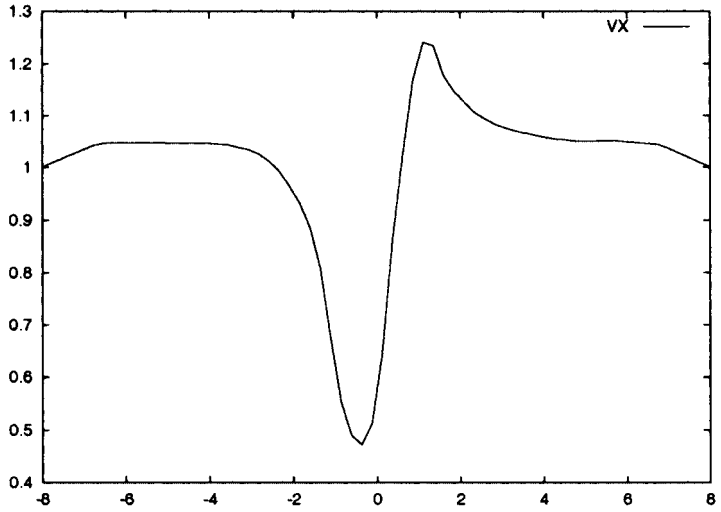

Figure 7. x-Component of the velocity at $x = 4$.

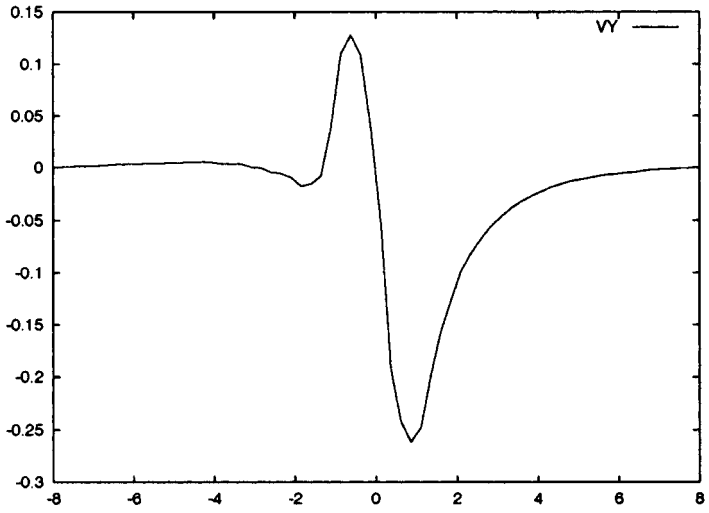

Figure 8. y-Component of the velocity at $x = 4$.

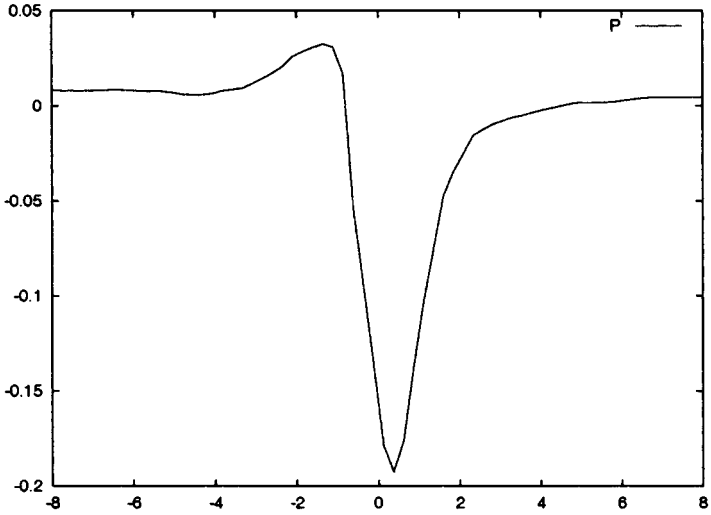

Figure 9. Pressure at $x = 4$.

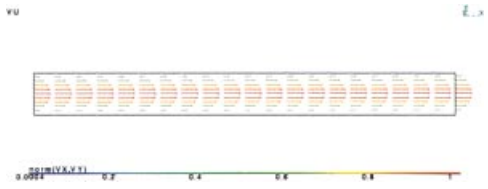

Plate 1. Velocity field $(Q_1 - P_0)$ element.

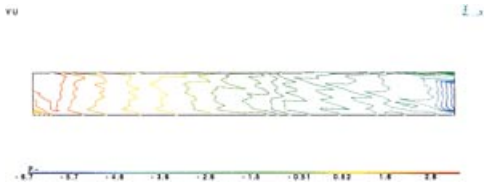

Plate 2. Pressure field, $(Q_1 - P_0)$ element.

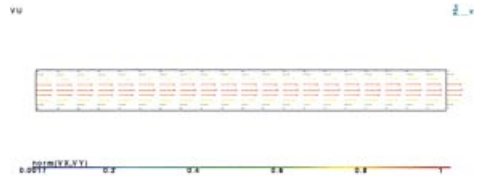

Plate 3. Velocity field, mini-element.

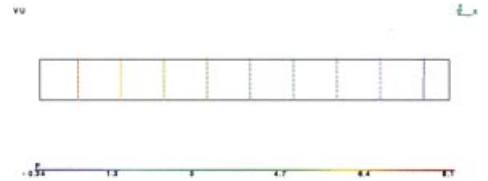

Plate 4. Pressure field, mini-element.

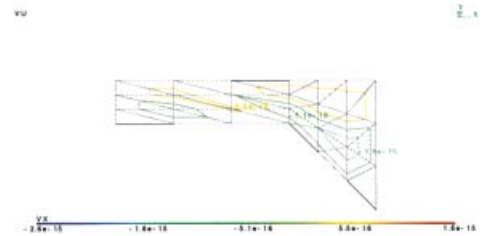

Plate 5. x-Component of velocity.

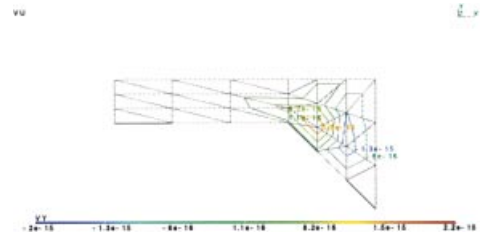

Plate 6. y-Component of velocity.

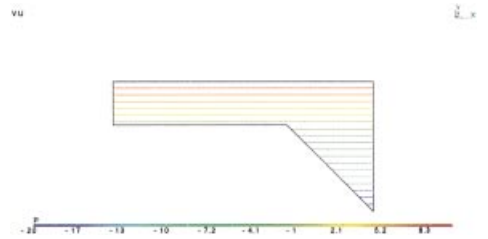

Plate 7. Pressure.

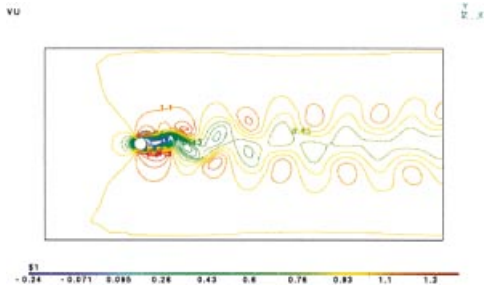

Plate 8. x-Component of the velocity.

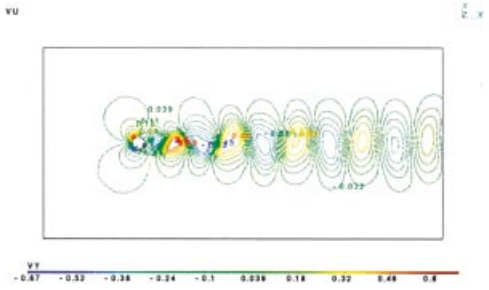

Plate 9. y-Component of the velocity.

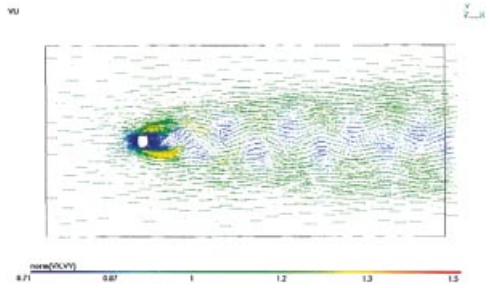

Plate 10. Velocity field.

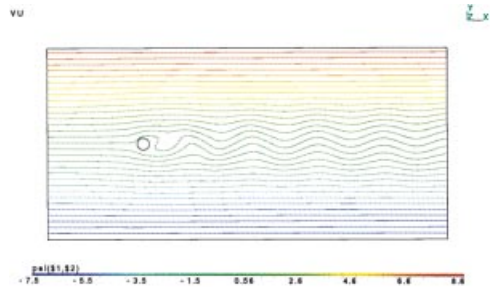

Plate 11. Streamline.

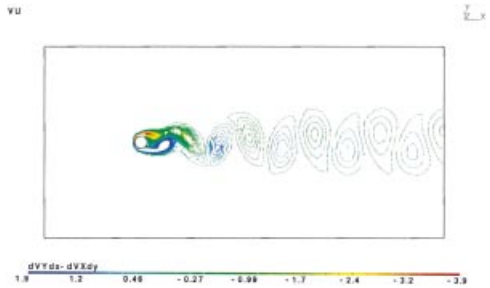

Plate 12. Vorticity.

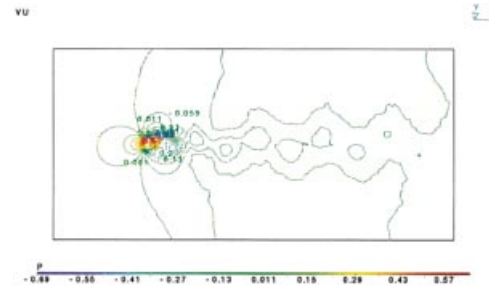

Plate 13. Pressure.

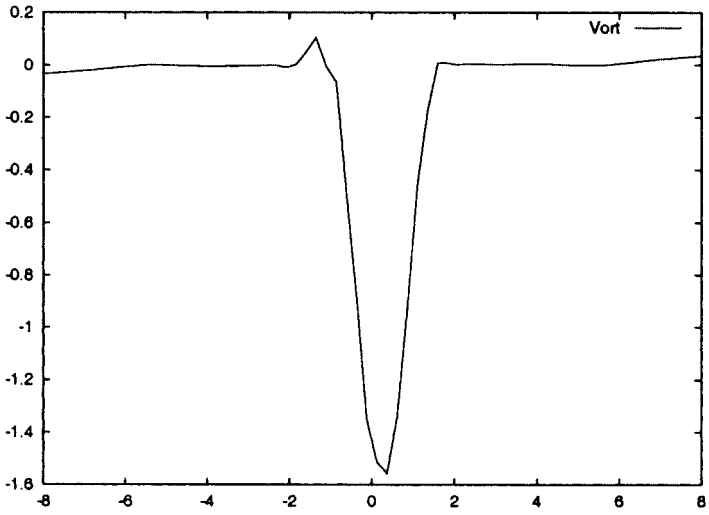

Figure 10. Vorticity at $x = 4$.

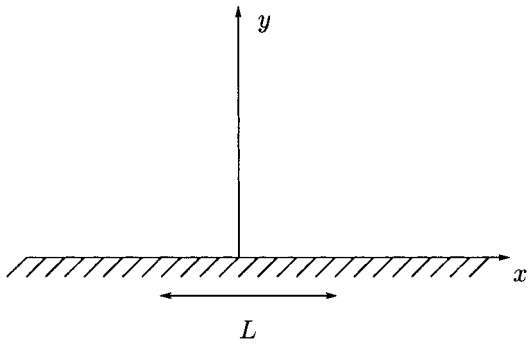

Figure 11. Oscillating plate.

a particular instant. In agreement with [47], this time t_{ref} was chosen to be the instant when the y-component of the velocity was changing from a negative to a positive value at the point ($x = 4$, $y = 0$). The solution at this time was interpolated using linear interpolation between the two bracketing time step solutions. Finally, Figures 7–10 are the values of various quantities at t_{ref}. All these results are in good agreement with the benchmark solution [47] and with other published solutions (see [48–51]) and show the vortex-shedding as expected.

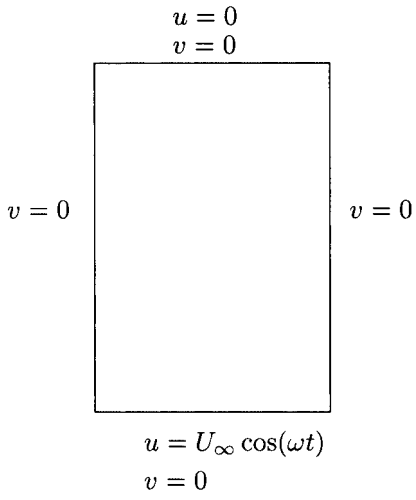

Figure 12. Computational domain and boundary conditions.

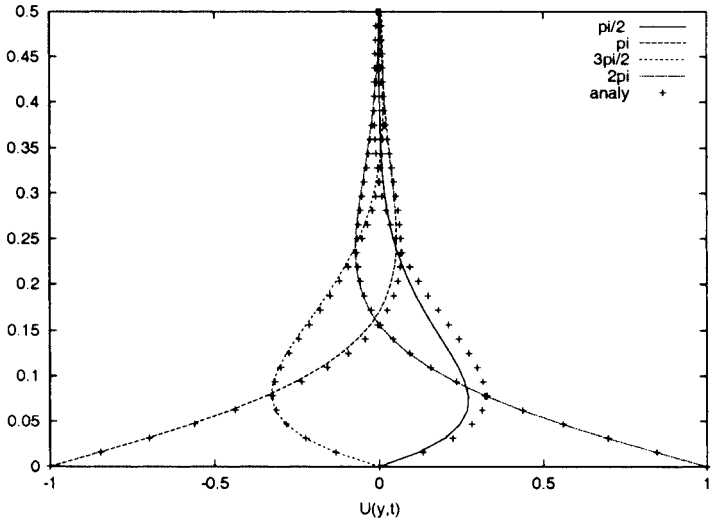

Figure 13. First cycle.

5.5. Stokes's second problem

We now consider the flow of an incompressible fluid over the two-dimensional plate subject to a planar oscillatory movement along the x-axis (see Figure 11). A harmonic damped oscillating velocity profile and a null pressure gradient solution of the analytic problem exists. The test case involved a simulation flow over a moving domain. The displacement of the plate is handled by a deformation of the grid and the domain in the temporal co-ordinate, which in this case is a uniform translation of the grid in the x-direction.

Figure 12 illustrates the computational domain and the boundary conditions. The Reynolds number is defined by $Re = U_\infty L/\nu$, L is the longitudinal displacement of the plate, U_∞ is maximum amplitude of the plate velocity, and $(\omega = 2\pi)$ is the oscillation frequency. Since, $U_\infty = 1$ and $L = 1/\pi$, ν is set to $1/10\pi$ in order to achieve a Reynolds numbers of 10. A complete description of this problem can be found in [52].

The mesh used for this simulation was refined near the bottom wall to capture the main features of the flow. The results presented here were obtained after three cycles (300 times steps with a fixed time step set to 0.01). In order to compare the computed and the analytical solutions, we report the x-component velocity profile at each quarter-cycle. Figures 13 and 14 are the comparaison of the solutions during the first and the second cycle respectively (the third cycle is identical to the second). The agreement with the analytical solution is very good except for the first quarter of the first cycle where the computed solution is not in phase since to start the computation a null initial condition was used.

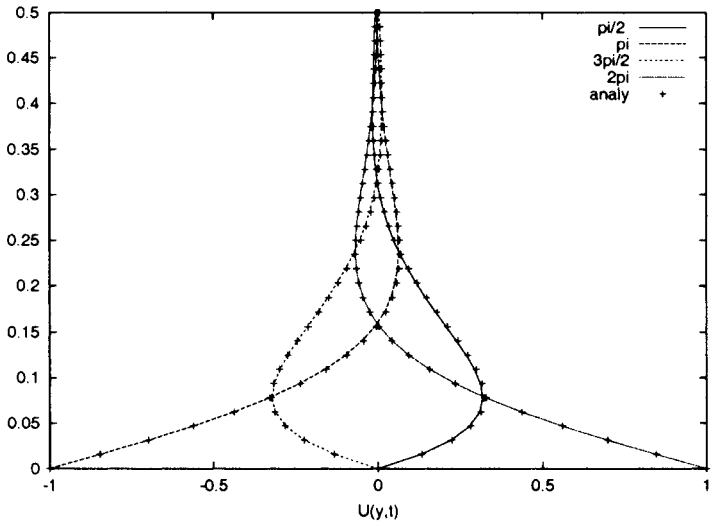

Figure 14. Second cycle.

26. CONCLUSIONS

A stable, mixed space–time formulation has been presented for the Navier–Stokes equations. The method is based on the time-discontinuous Galerkin formulation with the space–time mini-element. The velocity is linear, enriched with a piecewise linear bubble function, while the pressure is linear. The numerical results presented above confirm that the element is stable with respect to the inf–sup condition and that our procedure is capable of solving transient flows.

ACKNOWLEDGMENTS

This work was sponsored in part by the Natural Science and Engineering Research Council (NSERC) of Canada and the Fonds pour la Formation de Chercheurs et l'Aide à la Recherche (FCAR) of Quebec.

REFERENCES

1. Fried I. Finite-element analysis of time dependent phenomena. *AIAA Journal* 1969; **7**: 1170–1172.
2. Oden JT. A general theory of finite element, part I and part II. *International Journal for Numerical Methods in Engineering* 1969; **1**: 205–221, 247–259.
3. Bonnerot R, Jamet P. A second-order finite element method for the one-dimensional Stefan problem. *International Journal for Numerical Methods in Engineering* 1974; **8**: 811–820.
4. Bonnerot R, Jamet P. Numerical computation of the free boundary for the two-dimensional Stefan problem by space–time finite elements. *Journal of Computational Physics* 1977; **25**: 163–181.
5. Jamet P. Galerkin-type approximations which are discontinuous in time for the parabolic equations in a variable domain. *Journal of Computational Physics* 1978; **15**(5): 912–928.
6. Bonnerot R, Jamet P. A third order acurate discontinuous finite element method for the one dimensional Stefan problem. *Journal of Computational Physics* 1979; **25**: 145–167.
7. Hulbert GM, Hughes TJR. Space–time finite element methods for second-order hyperbolic equations. *Computer Methods in Applied Mechanics and Engineering* 1990; **84**: 327–348.
8. Li XD, Wiberg NE. Implementation and adaptivity of a space–time finite element method for structural dynamics. *Computer Methods in Applied Mechanics and Engineering* 1998; **156**: 221–229.
9. Wiberg N-E, Li X-D. Adaptive finite element procedures for linear and non-linear dynamics. *International Journal for Numerical Methods in Engineering* 1999; **46**: 1781–1802.
10. Thompson LL, Pinsky PM. A space–time finite element method for the exterior structural acoustics problem: time-dependent radiation boundary conditions in two space dimensions. *International Journal for Numerical Methods in Engineering* 1996; **39**: 1635–1657.
11. Thompson LL, Pinsky PM. A space–time finite element method for the structural acoustics in infinite domains part 2: Exact time-dependent non-reflecting boundary conditions. *International Journal for Numerical Methods in Engineering* 1996; **132**: 229–258.
12. Thompson LL, Pinsky PM. A space–time finite element method for the structural acoustics in infinite domains part 1: Formulation, stability and convergence. *International Journal for Numerical Methods in Engineering* 1996; **132**: 195–227.
13. Varoglu E, Liam Finn WD. Space–time finite elements incorporating characteristics for one-dimensional diffusion-convection equation. *Journal of Computational Physics* 1980; **34**: 371–389.
14. Varoglu E, Liam Finn WD. Utilisation of the method of characteristics to solve accurately two-dimensional transport problems by finite elements. *International Journal for Numerical Methods in Fluids* 1982; **2**: 173–184.
15. Johnson C, Saranen J. Streamline diffusion methods for the incompressible Euler and Navier–Stokes equations. *Mathematics of Computation* 1986; **47**: 1–18.
16. Hansbo P, Szepessy A. A velocity-pressure streamline diffusion finite element method for the incompressible Navier–Stokes equations. *Computer Methods in Applied Mechanics and Engineering* 1990; **84**: 175–192.
17. Tezduyar TE, Behr M. A new strategy for finite element computations involving moving boundaries and interfaces. The deforming-spatial-domain/space–time procedure: I. The concept and preliminary numerical tests. *Computer Methods in Applied Mechanics and Engineering* 1992; **94**: 339–351.

18. Tezduyar TE, Behr M. A new strategy for finite element computations involving moving boundaries and interfaces. The deforming-spatial-domain/space–time procedure: II. Computation of free-surface flow, two-liquid flows, and flows with drifting cylinders. *Computer Methods in Applied Mechanics and Engineering* 1992; **94**: 353–371.
19. Ladyshenskaya OA. *The Mathematical Theory of Viscous Incompressible Flows*. Gordon and Breach: New York, 1969.
20. Babuška I. The finite element method with Lagrangian multipliers. *Numerische Mathematik* 1973; **20**: 179–192.
21. Brezzi F. On the existence, uniqueness and approximation of saddle-point problems arising from Lagrange multipliers. *RAIRO Analyse Numérique* 1974; **R2**: 129–151.
22. Hughes TJR, Franca LP, Balestra M. A new finite element formulation for computational fluid dynamics. V. Circumventing the Babuška–Brezzi condition: A stable Petrov–Galerkin formulation of the Stokes problem accommodating equal-order interpolations. *Computer Methods in Applied Mechanics and Engineering* 1986; **59**: 85–99.
23. Eriksson K, Johnson C, Thomee V. Time discretisation of the parabolic problems by the discontinuous Galerkin method. *RAIRO Modelisation Mathematique et Analyse Numerique* 1985; **19**: 611–643.
24. Eriksson K, Johnson C. Error estimates and automatic time step control for nonlinear parabolic problems, *I**. *SIAM Journal of Numerical Analysis* 1987; **24**: 12–23.
25. Makridakis CG, Babuška I. On the stability of the discontinuous Galerkin method for the heat equation. *SIAM Journal of Numerical Analysis* 1997; **34**(1): 389–401.
26. Johnson C. Discontinuous Galerkin finite element methods for second order hyperbolic problems. *Computer Methods in Applied Mechanics and Engineering* 1993; **107**: 117–129.
27. Eriksson K, Johnson C. Adaptative finite element methods for parabolic problems I: A linear model problem. *SIAM Journal of Numerical Analysis* 1991; **28**: 43–77.
28. Johnson C. Error estimates and adaptive time-step control for a class of one-step methods for stiff ordinary differential equations. *SIAM Journal of Numerical Analysis* 1988; **25**(4): 908–926.
29. Froncioni AM, Labbe P, Garon A, Camarero R. Interpolation-free space–time remeshing for the Burger's equation. *Communication in Numerical Methods in Engineering* 1997; **13**: 875–884.
30. Masud A, Hughes TJR. A space–time Galerkin/least-squares finite element formulation of the Navier–Stokes equations for moving domain problems. *Computer Methods in Applied Mechanics and Engineering* 1997; **146**: 91–126.
31. Varoglu E, Liam Finn WD. Space–time finite elements incorporating characteristics for the Burger's equation. *International Journal for Numerical Methods in Engineering* 1980; **16**: 174–184.
32. Johnson C. The characteristic streamline diffusion method. *Matematica Aplicada e Computacional* 1991; **10**: 229–242.
33. Hansbo P. The characteristic streamline diffusion method for convection-diffusion problems. *Computer Methods in Applied Mechanics and Engineering* 1992; **96**: 239–253.
34. Hansbo P. The characteristic streamline diffusion method for time-dependent incompressible Navier–Stokes equations. *Computer Methods in Applied Mechanics and Engineering* 1992; **99**: 171–186.
35. Hansbo P. The characteristic streamline diffusion method for incompressible flow in three dimensions. In *8th International Conference on Finite Elements in Fluids*. Pineridge Press: Swansea, 1993; 287–295.
36. Hansbo P. Lagrangian incompressible flow computations in three dimensions by the use of space–time finite elements. *International Journal for Numerical Methods in Fluids* 1995; **20**: 989–1001.
37. Pironneau O, Liou J, Tezduyar T. Characteristic-Galerkin and Galerkin/least-squares space–time formulations for the advection-diffusion equation with time-dependent domains. *Computer Methods in Applied Mechanics and Engineering* 1992; **100**: 117–141.
38. Brezzi F, Fortin M. *Mixed and Hybrid Finite Element Methods*. Springer-Verlag: New York, 1991.
39. Arnold DN, Brezzi F, Fortin M. A stable finite element for the Stokes equations. *Calcolo* 1984; **21**: 337–344.
40. Fortin A. Méthode d'éléments finis pour les équations de Navier–Stokes. PhD thesis, Université Laval, 1984.
41. Clément P. Approximation by finite element functions using local regularization. *RAIRO Analyse Numerique* 1975; **9**: 77–84.
42. Bernardi C. Optimal finite-element interpolation on curved domains. *SIAM Journal of Numerical Analysis* 1989; **26**(5): 1212–1240.
43. Bernardi C, Girault. V. A local regularization operator for triangular and quidrilateral finite elements. *SIAM Journal on Numerical Analysis* 1998; **35**(5): 1893–1916.
44. Dupont T, Scott LR. Polynomial approximation of functions in Sobolev spaces. *Mathematics of Computation* 1980; **34**: 441–463.
45. Fortin M, Fortin A. Experiments with several elements for incompressible flows. *International Journal for Numerical Methods in Fluids* 1985; **5**: 911–928.

46. Gresho PM, Lee RL, Sani RL. Further studies in equal order interpolation for Navier–Stokes. In *Fifth International Symposium on Finite Elements in Flow Problems*, Austin, Texas, 1984; 143–148.
47. Engelman MS, Jaminia M-A. Transient flow past a circular cylinder: A benchmark solution. *International Journal for Numerical Methods in Fluids* 1990; **11**: 985–1000.
48. Behr M, Liou J, Shih R, Tezduyar TE. Vorticity-streamfunction formulation of the unsteady incompressible flow past a cylinder: sensibility of the computed flow field to the location of the outflow boundary. *International Journal for Numerical Methods in Fluids* 1991; **12**: 323–342.
49. Tezduyar TE, Mittal S, Ray SE, Shih R. Incompressible flow computations with stabilized bilinear and linear equal-order-interpolation velocity-pressure elements. *Computer Methods in Applied Mechanics and Engineering* 1992; **95**: 221–242.
50. Behr M, Hastreiter D, Mittal S, Tezduyar TE. Incompressible flow past a circular cylinder: dependence of the computed flow field on the location of the lateral boundaries computations with stabilized bilinear and linear equal-order-interpolation velocity-pressure elements. *Computer Methods in Applied Mechanics in Engineering* 1995; **123**: 309–316.
51. Codina R, Blasco J. Stabilized finite element method for the transient Navier–Stokes equations based on a pressure gradient projection. *Computer Methods in Applied Mechanics and Engineering* 2000; **182**: 277–300.
52. Ryhming IL. *Dynamique des Fluides*. Presses Polytechnique Romandes: Lausanne, 1985.

